Estimating the ground-state hyperfine shifts of group-1 atoms due to long-range collisions, static electric fields, and nearby surfaces

B. H. McGuyer
National Coalition of Independent Scholars, Glastonbury, Connecticut 06033, USA

K. Choksi, N. VonHeeder, and B. A. Olsen*
Department of Physics, Lewis & Clark College, Portland, Oregon 97219, USA

(Received 28 August 2026; accepted 19 October 2026; published 3 November 2026)

Many interactions perturb (or shift) the hyperfine coupling in group-1 atoms between their nuclear spin and single valence electron. Previous work provided an approach to estimate this shift from electric-dipole interactions both during nonreactive collisions with other atoms or molecules at long range and with static electric fields. We extend this approach to estimate the shift due to a nearby conductive surface and improve all these estimates by numerically computing updated values for the characteristic energies they use. We investigate how to estimate these energies by scaling arguments and suggest how to adapt the approach to other applications. The results are relevant to pressure shifts in vapor cells, Stark shifts, and wall shifts in nanoscale devices.

DOI: 10.1103/7c32-zttg

I. INTRODUCTION

In group-1 atoms (hydrogen and the alkali metals), the hyperfine coupling $A_g\mathbf{I}\cdot\mathbf{S}$ between the spin $\mathbf{I}$ of the nucleus and the spin $\mathbf{S}$ of the single valence electron leads to energy splittings of the ground state corresponding to microwave frequencies. These hyperfine frequencies form the basis for many atomic frequency standards (or clocks) and for the current SI definition of the second [1,2]. Transitions between ground-state sublevels in alkali-metal atoms split by these frequencies find wide use in quantum metrology [3] and searches for new physics [4–7]. These and other hyperfine interactions allow laser spectroscopy to probe nuclear physics [8], enable sensing with nitrogen-vacancy centers in diamond [9,10], and play a critical role in silicon quantum electronics [11,12].

Shifts of these group-1 hyperfine frequencies are important to the accuracy, performance, and noise floor of many applications. For example, a common technique to improve clock signals is to add nonreactive buffer gases (often noble gases) to introduce collisions with alkali-metal atoms [13]. However, these collisions lead to a "pressure" shift and broadening of the clock transition, and are the main reason why Rb clocks are secondary standards [2,14–17]. Accordingly, pressure shifts have received significant attention over the past several decades.

For the ground state, the shift follows the change in the value of the wave function for the group-1 valence electron evaluated at the nucleus, or $\psi_{gS}(0)$, as illustrated in Fig. 1. Previous work studying collisions and the pressure shift found a simple approach to estimate the shift δA_g of the coupling

*Contact author: bolsen@lclark.edu; https://olsenlab.science

Published by the American Physical Society under the terms of the Creative Commons Attribution 4.0 International license. Further distribution of this work must maintain attribution to the author(s) and the published article's title, journal citation, and DOI.

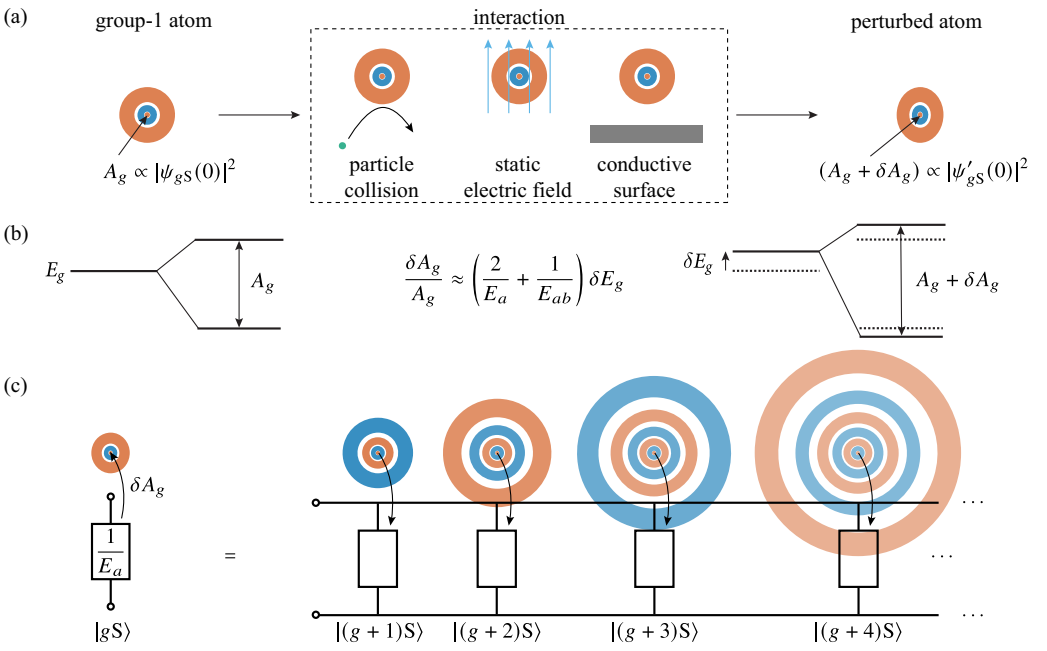


FIG. 1. Conceptual picture of hyperfine shifts for a group-1 atom following the form of Eq. (1). (a) When a group-1 atom in its ground state is perturbed by an interaction, such as those illustrated here, the valence electronic wave function changes shape (conceptually sketched for Na). If the probability for the valence electron to be at the nucleus changes, then the hyperfine coupling coefficient A_g shifts by a corresponding amount δA_g. (b) For shifts following the form of Eq. (1), which is repeated here, this shift depends on the overall perturbation δE_g as well as the two energies E_a and E_{ab}. (c) The first energy, E_a, only depends on properties of the group-1 atom, so is characteristic of that atom. The value of E_a comes from a sum over all nS states [see Eq. (5)], with contributions from each excited S-state coupling A_n adding in parallel.

A_g at large collision distances [2,18,19], which has the form

$$\frac{\delta A_g}{A_g} \approx \left(\frac{2}{E_a} + \frac{1}{E_{ab}}\right)\delta E_g. \tag{1}$$

Here, E_a is a "characteristic" energy that depends only on the group-1 atom, E_{ab} is a smaller correction that depends on the colliding pair, and δE_g is the collisional perturbation of the ground-state energy E_g. This form is valid only at large internuclear separations R between the colliding pair, where retardation is negligible. More generally, both δA_g and δE_g are functions of R, and $\delta E_g(R)$ is the interaction potential for the pair. The full potential $\delta A_g(R)$ is important to the pressure shift [20–23], as well as alkali-metal–noble-gas van der Waals molecules [24–26] and magnetoassociation [27–29].

The original estimates of the energies E_a and E_{ab} in Eq. (1) were fairly crude, such as $E_a \approx \overline{E}_e$ (the mean of certain excited-state energies) [2] or $E_a \approx E_\infty$ (the ionization energy) [19]. In previous work, we calculated improved values of E_a for Na, K, Rb, and Cs using perturbation theory and gave an explicit formula for the accompanying values of E_{ab} [30]. Additionally, we extended the approach to estimate hyperfine Stark-shift coefficients k due to static electric fields and tested our values for E_a by comparing to experimental results. Such shifts are important systematics in precision measurements, and many values of k are well known due to their importance to black-body radiation (BBR) shifts in atomic clocks [31,32].

In this paper, we extend the approach behind Eq. (1) to a new application, the shift from a nearby conductive surface, and extend our calculation of the characteristic energies E_a to all group-1 atoms, by including H, Li, and Fr. Using recently expanded experimental results [33], as well as some improvements to our numerical methods, this provides updated values for Na–Cs. As in our previous work, we compute Stark-shift coefficients k, now for all group-1 atoms, and compare with experimental results. We additionally bolster our results with a scaling argument relating E_a to the splitting E_S between the ground and first excited S states of the group-1 atom.

Our extension to estimate the ground-state hyperfine shifts due to a nearby surface (or wall) treats the van der Waals regime [34] of the dispersion forces [35] between a group-1 atom and the surface. This regime applies when the separation R from the surface is large enough to treat the force as that between the atom and the image charges it induces in a conductor, but small enough to ignore retardation [36] and the resulting Casimir-Polder regime [35]. These surface interactions are receiving increased scrutiny because the size of atomic devices continues to decrease [37,38]. In particular, hyperfine shifts in miniature vapor cells [39–41], in hollow-core fibers [42], or near micromachined waveguides [43] can affect spectroscopic measurements and sensor performance.

This paper is organized as follows: Section II outlines how interactions can produce shifts with the form of Eq. (1) through either second- or third-order perturbations. We treat three specific applications in detail: wall shifts from nearby conductive surfaces, pressure shifts from long-range collisions, and Stark shifts from static electric fields. Section III outlines our approach to estimate the characteristic energy E_a using both numerical calculation and scaling arguments. Section IV reports our results for E_a as well as additional quantities for the three specific applications. Section V discusses these results and possible future work and extensions. Section VI concludes the paper, and the Appendix provides reference values for group-1 atoms. Our numerical code is available online, along with intermediate calculations and plots [44].

II. BACKGROUND

Following Refs. [30,45], consider a group-1 atom perturbed by an interaction $W = H_{\rm hf} + U$ that is the sum of the contact magnetic-dipole hyperfine interaction of that atom [33,46],

$$H_{\rm hf} = \frac{8\pi}{3} g_S \mu_B \frac{\mu_I}{I} \delta(\mathbf{r})\, \mathbf{I}\cdot\mathbf{S}, \tag{2}$$

and an interaction U with an external perturbation. Here, g_S is the g factor corresponding to the group-1 valence electronic spin $\mathbf{S}$, μ_B is the Bohr magneton, μ_I is the nuclear magneton corresponding to the group-1 nuclear spin $\mathbf{I}$ with spin quantum number I, and $\mathbf{r}$ is the displacement of the group-1 single valence electron from the nucleus. Below, we will use U to model an interaction with another particle during a collision, an external electric field, or a nearby surface. To handle all three cases, let us proceed by assuming a colliding partner and denoting the state of the colliding pair as $|\mu\nu\rangle = |\mu\rangle_a \otimes |\nu\rangle_b$, with the group-1 atom "a" in eigenstate μ and perturbing particle "b" in state ν, with corresponding energy $E_{\mu\nu}$, and joint ground state $|00\rangle$. The cases without a colliding partner follow by setting $\nu = 0$ and using $\langle 0\,|\,0\rangle_b = 1$.

From time-independent perturbation theory, the first-order energy shift of the ground state due to W is

$$\delta E_{00,1} = \langle 00|W|00\rangle = \langle 00\,|\,H_{\rm hf}\,|\,00\rangle + \langle 00\,|\,U\,|\,00\rangle = \delta E^{\rm (hf)}_{00,1} + \delta E^{(U)}_{00,1}, \tag{3}$$

where the first term is the hyperfine energy

$$\delta E^{\rm (hf)}_{00,1} = \langle 00\,|\,H_{\rm hf}\,|\,00\rangle = \langle 0\,|\,H_{\rm hf}\,|\,0\rangle_a \otimes \langle 0\,|\,0\rangle_b = A_g \langle \mathbf{I}\cdot\mathbf{S}\rangle_a, \tag{4}$$

with a magnetic-dipole hyperfine coupling coefficient A_g for the group-1 atom in the ground (or "g") S state. Here, and subsequently, let us use g to denote the value of the principal quantum number n for the ground state. The value of A_g is proportional to the probability density for the valence electron

to be at the nucleus: $A_g \propto |\psi_{gS}(0)|^2$. In what follows, we will denote ground-state expectations of operators X as $\langle X\rangle_a$ or $\langle X\rangle_b$, and occasionally omit the subscripts "a" and "b" for clarity.

Section II A treats the case when the second term $\delta E^{(U)}_{00,1} = \langle 00 \,|\, U \,|\, 00\rangle \neq 0$, which leads to a second-order hyperfine perturbation, and Sec. II B treats the case of $\delta E^{(U)}_{00,1} = 0$, which leads to a third-order hyperfine perturbation. In both cases, we show that the resulting shifts involve a characteristic energy E_a given by

$$\frac{1}{E_a} = \sum_{n>g} \frac{\langle gS \,|\, H_{\rm hf} \,|\, nS\rangle\langle nS \,|\, r^2 \,|\, gS\rangle}{\langle H_{\rm hf}\rangle(E_g - E_n)\langle r^2\rangle} \approx \sum_{n>g} \left(\frac{\sqrt{|A_n/A_g|}}{E_g - E_n}\right) \frac{\langle nS \,|\, r^2 \,|\, gS\rangle}{\langle gS \,|\, r^2 \,|\, gS\rangle} > 0. \tag{5}$$

Here, the sum is over all excited nS states of the group-1 atom with corresponding energies E_n and magnetic-dipole coupling coefficients A_n, and includes the ground state gS and ground-state energy E_g. The second form follows from the square-root formula $\langle gS \,|\, H_{\rm hf} \,|\, nS\rangle \approx \sqrt{\langle nS \,|\, H_{\rm hf} \,|\, nS\rangle\langle H_{\rm hf}\rangle}$, which group-1 atoms are expected to satisfy within a percent [47,48]. This characteristic energy, which was originally derived in the context of collision shifts [2,30,45], depends only on the properties of the group-1 atom. Notably, this definition is independent of the perturbing potential U. As indicated, this energy evaluates to a positive quantity because the signs of the calculated elements $\langle nS \,|\, r^2 \,|\, gS\rangle$ are negative, as are the energy differences $E_g - E_n$. This sign can also be justified by assuming a negligible contribution from energies above a cutoff, such that we can substitute $E_n - E_g \leqslant E_{\rm cut} > 0$ in the first form, then adding and subtracting an $n = g$ term, using closure to remove the sum, and noting $\delta(r)r^2 = 0$, which gives $1/E_a \geqslant 1/E_{\rm cut} > 0$.

A. Second-order hyperfine perturbations

For the case of $\delta E^{(U)}_{00,1} \neq 0$, and generalizing the approach in Ref. [45], consider the second-order perturbation to the colliding pair ground-state energy,

$$\delta E_{00,2} = \sum_{\mu\nu\neq 00} \frac{|\langle 00 \,|\, W \,|\, \mu\nu\rangle|^2}{E_{00} - E_{\mu\nu}}, \tag{6}$$

which is a sum over all states but the joint ground state $|\mu\nu\rangle = |00\rangle$. For small U, the leading-order perturbation comes from terms linear in both $H_{\rm hf}$ and U (note the combinatorial factor of 2):

$$\delta E^{(\rm lin)}_{00,2} = 2\sum_{\mu\nu\neq 00} \frac{\langle 00 \,|\, H_{\rm hf} \,|\, \mu\nu\rangle\langle \mu\nu \,|\, U \,|\, 00\rangle}{E_{00} - E_{\mu\nu}} = 2\sum_{\mu>0} \frac{\langle 00 \,|\, H_{\rm hf} \,|\, \mu 0\rangle\langle \mu 0 \,|\, U \,|\, 00\rangle}{E_{00} - E_{\mu 0}}. \tag{7}$$

The second form follows from $H_{\rm hf}$ acting only on the group-1 atom. Note that the only nonzero contributions are from group-1 nS states; $\langle 00 \,|\, H_{\rm hf} \,|\, \mu 0\rangle \propto \langle 0 \,|\, \delta(\mathbf{r}) \,|\, \mu\rangle_a = 0$ for all other states. Thus, in what follows, we will use the integers g, n, and corresponding sums, to denote the ground gS and excited nS states for the group-1 atom. Next, consider interactions that satisfy (or are well approximated by) the relation

$$\frac{\langle \mu 0 \,|\, U \,|\, 00\rangle}{\langle 00 \,|\, U \,|\, 00\rangle} = \frac{\langle \mu 0 \,|\, r_a^2 \,|\, 00\rangle}{\langle 00 \,|\, r_a^2 \,|\, 00\rangle} \approx \frac{\langle \mu 0 \,|\, r^2 \,|\, 00\rangle}{\langle 00 \,|\, r^2 \,|\, 00\rangle} \tag{8}$$

for nS states, where $r_a = |\mathbf{r}_a|$, $\mathbf{r}_a = \mathbf{r} + \mathbf{r}_c$ is the sum of all group-1 electron positions, $\mathbf{r}_c = \sum_i \mathbf{r}_{c,i}$ is the sum of all group-1 core electron positions, and $r = |\mathbf{r}|$, all relative to the group-1 nucleus. Then, we have

$$\begin{aligned}\delta E^{(\rm lin)}_{00,2} &\approx 2\langle 00 \,|\, U \,|\, 00\rangle \sum_{n>g} \frac{\langle g \,|\, H_{\rm hf} \,|\, n\rangle\langle n \,|\, r^2 \,|\, g\rangle}{(E_{g0} - E_{n0})\langle r^2\rangle} \\ &= 2\delta E^{(U)}_{00,1}\langle H_{\rm hf}\rangle \sum_{n>g} \frac{\langle g \,|\, H_{\rm hf} \,|\, n\rangle\langle n \,|\, r^2 \,|\, g\rangle}{\langle H_{\rm hf}\rangle(E_{g0} - E_{n0})\langle r^2\rangle} = \delta E^{(U)}_{00,1}\delta E^{(\rm hf)}_{00,1}\left(\frac{2}{E_a}\right),\end{aligned} \tag{9}$$

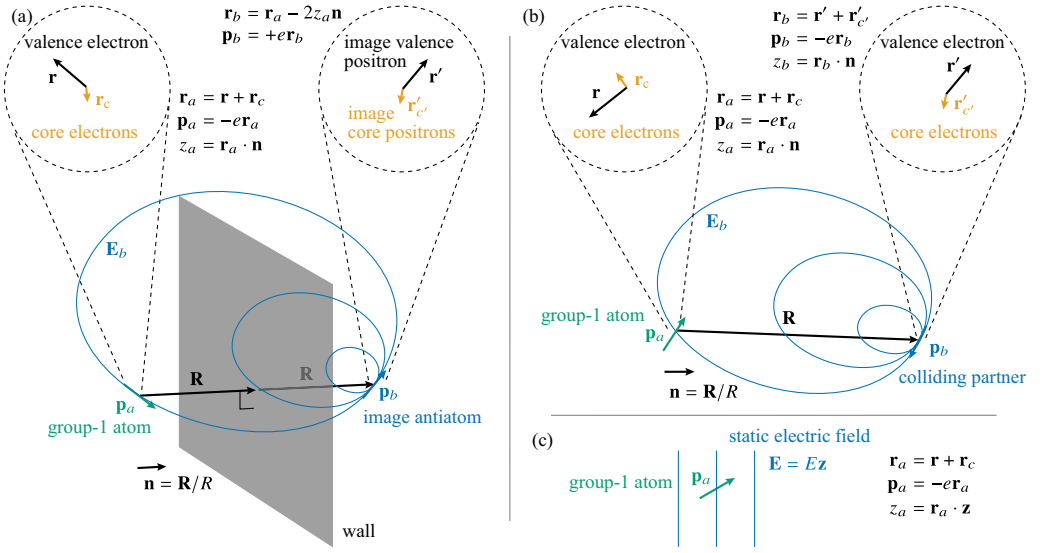


FIG. 2. Diagrams for applications in Sec. II. (a) Wall shift from a nearby conductive surface. The group-1 atom at a distance $\mathbf{R}$ from the wall induces an image antiatom $2\mathbf{R}$ away. The image antiatom has instantaneous electric-dipole moment $\mathbf{p}_b$, producing an electric field $\mathbf{E}_b$ that interacts with the atom's moment $\mathbf{p}_a$. (b) Pressure shift from a long-range collision. The partner's instantaneous electric-dipole moment $\mathbf{p}_b$ produces an electric field $\mathbf{E}_b$ that interacts with the group-1 atom's moment $\mathbf{p}_a$. (c) Stark shift from a static electric field. We define coordinates so that $\mathbf{E} = E\mathbf{z}$. All notation is defined in the text.

which recovers the characteristic energy E_a of Eq. (5). This allows us to write the fractional ground-state hyperfine shift in the form of Eq. (1) as

$$\frac{\delta A_g}{A_g} \approx \frac{\delta E^{(\mathrm{lin})}_{00,2}}{\delta E^{(\mathrm{hf})}_{00,1}} = \left(\frac{2}{E_a}\right)\delta E^{(U)}_{00,1}. \tag{10}$$

The only requirements for this result are (1) that $\langle 00\,|\,U\,|\,00\rangle \neq 0$ and (2) that the relationship in Eq. (8) holds.

Before we continue, note that, somewhat surprisingly, this result does not include the E_{ab} term present in Eq. (1). As a result, if U models a collision, for example, then any relevant properties of the collision partner would only contribute via $\delta E^{(U)}_{00,1}$. Our treatment of collisions below does not satisfy the requirements for this form, since $\langle 00\,|\,U\,|\,00\rangle = 0$ for that application. However, as noted in Ref. [30], an effective operator can be constructed that does satisfy the requirements for this form, as shown in Sec. II B, which can be used to model collisions or other interactions. Therefore, care is needed using such effective operators because they neglect the E_{ab} term.

Wall shift from a nearby surface

One example of a shift with the form of Eq. (10) is the interaction of a group-1 atom with a nearby conducting wall [cf. complement $\mathrm{C_{XI}}$ part 4 of Ref. [49], as depicted in Fig. 2(a)]. Consider a group-1 atom at position $\mathbf{x}_a$, which is a normal distance $\mathbf{R}$ away from a flat, perfectly conducting surface, with $\mathbf{n} = \mathbf{R}/|\mathbf{R}|$ the unit vector pointing from the atom toward the closest point on the surface. The atom induces surface charges that produce an electric field equivalent to an image antiatom at position $\mathbf{x}_b = \mathbf{x}_a + 2\mathbf{R}$. Assuming the distance $R = |\mathbf{R}|$ is large enough to neglect details of the surface, but small enough to neglect retardation effects [36], the leading-order interaction in

U has a dispersive van der Waals form given by

$$U_S = -\tfrac{1}{2}\mathbf{p}_a \cdot \mathbf{E}_b(\mathbf{x}_a), \tag{11}$$

where $\mathbf{p}_a = -e\mathbf{r}_a$ is the instantaneous electric-dipole moment of the atom, $\mathbf{E}_b$ is the electric field produced by the image, and the coefficient $\frac{1}{2}$ removes the fictitious energy behind the wall. The field $\mathbf{E}_b(\mathbf{x}_a) = (3\mathbf{nn} - \mathbb{1}) \cdot \mathbf{p}_b/(2R)^3$, where $\mathbb{1}$ is the identity dyadic tensor and $\mathbf{p}_b = +e\mathbf{r}_b$ is the instantaneous electric-dipole moment of the image antiatom. As sketched in Fig. 2 (a), the sum of all antiatom electronic positions $\mathbf{r}_b = \mathbf{r}_a - 2z_a\mathbf{n}$, where the normal projection $z_a = \mathbf{r}_a \cdot \mathbf{n}$. Together, this gives

$$U_S = \frac{e^2}{2}\left[\frac{\mathbf{r}_a \cdot (3\mathbf{nn} - \mathbb{1}) \cdot (\mathbf{r}_a - 2z_a\mathbf{n})}{8R^3}\right] = \frac{-e^2}{16R^3}\left(r_a^2 + z_a^2\right). \tag{12}$$

Noting that $\langle U_S\rangle \neq 0$ and that $\langle n \,|\, z_a^2 \,|\, g\rangle = \frac{1}{3}\langle n \,|\, r_a^2 \,|\, g\rangle$ by symmetry for nS states, we see that both required conditions are satisfied for the result of Eq. (10). Rewriting the first-order perturbation as $\delta E_{00,1}^{(U_S)} = \langle U_S\rangle = -C_3/R^3$, where

$$C_3 = e^2\langle r_a^2\rangle/12 \tag{13}$$

is the atom-surface dispersion coefficient C_3 of the ground-state group-1 atom [50], we can write the shift as

$$\frac{\delta A_{g,S}}{A_g} \approx -\left(\frac{2}{E_a}\right)\frac{C_3}{R^3}. \tag{14}$$

We estimate this "wall" (or "surface") shift in Sec. IV B for a representative distance R.

B. Third-order hyperfine perturbations

For the case of $\delta E_{00,1}^{(U)} = 0$, and generalizing the approach in Ref. [30], consider an interaction U that has a nonzero second-order perturbation,

$$\delta E_{00,2}^{(U)} = \sum_{\mu\nu\neq 00} \frac{|\langle 00 \,|\, U \,|\, \mu\nu\rangle|^2}{E_{00} - E_{\mu\nu}} \neq 0, \tag{15}$$

and that satisfies $\langle 00 \,|\, U \,|\, \mu 0\rangle = 0$ when μ is an nS state of the group-1 atom, say, from spherical symmetry. Then, the only nonvanishing terms of the total second-order perturbation $\delta E_{00,2}$ are quadratic in either $H_{\rm hf}$ or U, with no mixed terms linear in both. Instead, the third-order shift

$$\delta E_{00,3} = \sum_{\mu\nu\neq 00}\sum_{\eta\xi\neq 00} \frac{\langle 00 \,|\, W \,|\, \mu\nu\rangle\langle\mu\nu \,|\, W \,|\, \eta\xi\rangle\langle\eta\xi \,|\, W \,|\, 00\rangle}{(E_{00} - E_{\mu\nu})(E_{00} - E_{\eta\xi})} - \langle 00 \,|\, W \,|\, 00\rangle \sum_{\rho\sigma\neq 00} \frac{|\langle 00 \,|\, W \,|\, \rho\sigma\rangle|^2}{(E_{00} - E_{\rho\sigma})^2} \tag{16}$$

contains terms linear in $H_{\rm hf}$ (note the combinatorial factor of 2):

$$\delta E_{00,3}^{(\rm lin)} = 2\sum_{\mu\nu\neq 00}\sum_{\eta\xi\neq 00} \frac{\langle 00 \,|\, H_{\rm hf} \,|\, \mu\nu\rangle\langle\mu\nu \,|\, U \,|\, \eta\xi\rangle\langle\eta\xi \,|\, U \,|\, 00\rangle}{(E_{00} - E_{\mu\nu})(E_{00} - E_{\eta\xi})} - \langle 00 \,|\, H_{\rm hf} \,|\, 00\rangle \sum_{\rho\sigma\neq 00} \frac{|\langle 00 \,|\, U \,|\, \rho\sigma\rangle|^2}{(E_{00} - E_{\rho\sigma})^2}. \tag{17}$$

As before, we can simplify the first sum by noting that $H_{\rm hf}$ acts only on the group-1 atom, giving $\nu = 0$. To proceed, let us approximate the denominators with an effective energy scale $\hat{E}$ using the substitutions $(E_{00} - E_{\mu\nu})(E_{00} - E_{\eta\xi}) \approx -\hat{E}(E_{00} - E_{\mu\nu})$ and $(E_{00} - E_{\rho\sigma})^2 \approx -\hat{E}(E_{00} - E_{\rho\sigma})$. Then, we

can remove the next sum with the closure relation $\sum_{\eta\xi} |\eta\xi\rangle\langle\eta\xi| = 1$, noting $\langle 00|U|00\rangle = 0$ by assumption. Next, consider interactions that satisfy (or are well approximated by) the relation

$$\frac{\langle\mu 0|U^2|00\rangle}{\langle 00|U^2|00\rangle} = \frac{\langle\mu 0|r_a^2|00\rangle}{\langle 00|r_a^2|00\rangle} \approx \frac{\langle\mu 0|r^2|00\rangle}{\langle 00|r^2|00\rangle} \tag{18}$$

for nS states. Altogether, we then have

$$\begin{aligned}
\delta E_{00,3}^{(\mathrm{lin})} &\approx -2\langle 00|U^2|00\rangle \sum_{\mu\neq 0} \frac{\langle 00|H_{\mathrm{hf}}|\mu 0\rangle\langle\mu 0|r^2|00\rangle}{\hat{E}(E_{00}-E_{\mu\nu})\langle 00|r^2|00\rangle} + \delta E_{00,1}^{(\mathrm{hf})} \sum_{\rho\sigma\neq 00} \frac{|\langle 00|U|\rho\sigma\rangle|^2}{\hat{E}(E_{00}-E_{\rho\sigma})} \\
&= \left(\frac{1}{\hat{E}}\right)\left(-2\langle 00|U^2|00\rangle\langle H_{\mathrm{hf}}\rangle \sum_{\mu\neq 0} \frac{\langle 00|H_{\mathrm{hf}}|\mu 0\rangle\langle\mu 0|r^2|00\rangle}{\langle H_{\mathrm{hf}}\rangle(E_{00}-E_{\mu\nu})\langle r^2\rangle} + \delta E_{00,1}^{(\mathrm{hf})}\delta E_{00,2}^{(U)}\right) \\
&= \left(\frac{1}{\hat{E}}\right)\left(-\langle 00|U^2|00\rangle\frac{2}{E_a} + \delta E_{00,2}^{(U)}\right)\delta E_{00,1}^{(\mathrm{hf})},
\end{aligned} \tag{19}$$

which recovers the characteristic energy E_a of Eq. (5). The resulting fractional ground-state hyperfine shift is

$$\frac{\delta A_g}{A_g} \approx \frac{\delta E_{00,3}^{(\mathrm{lin})}}{\delta E_{00,1}^{(\mathrm{hf})}} \approx \left(\frac{1}{\hat{E}}\right)\left(-\langle 00|U^2|00\rangle\frac{2}{E_a} + \delta E_{00,2}^{(U)}\right), \tag{20}$$

which is similar to but not exactly of the same form as Eq. (1). This intermediate form is used below for calculating the Stark shift. Otherwise, lacking any particular motivation for choosing $\hat{E}$, we can choose a self-consistent value for which the approximation $E_{00} - E_{\rho\sigma} \approx -\hat{E}$ used above, together with closure, returns the $\delta E_{00,2}^{(U)}$ of Eq. (15) to itself. This self-consistent value for $\hat{E}$ is

$$E_{ab} = -\frac{\langle 00|U^2|00\rangle}{\delta E_{00,2}^{(U)}}. \tag{21}$$

After substituting this value for $\hat{E}$, the intermediate form of Eq. (20) recovers the form of Eq. (1):

$$\frac{\delta A_g}{A_g} \approx \left(\frac{2}{E_a} + \frac{1}{E_{ab}}\right)\delta E_{00,2}^{(U)}. \tag{22}$$

As before, the characteristic energy E_a depends only on properties of the group-1 atom, but here the "correction" energy E_{ab} depends on properties of both the atom and the perturbation. The only requirements for both this final result as well as the intermediate result of Eq. (20) are (1) that $\langle 00|U|00\rangle = 0$, (2) that $\delta E_{00,2}^{(U)} \neq 0$, (3) that $\langle 00|U|\mu 0\rangle = 0$ for nS states $|\mu\rangle_a$, and (4) that the relation in Eq. (18) holds.

Before we continue, let us return to the comment following Eq. (10) about E_{ab} being absent in the second-order result. Note that the effective operator $U' = \sum_{\mu\nu\neq 00} U|\mu\nu\rangle\langle\mu\nu|U/(E_{00}-E_{\mu\nu})$, which could come from a Van Vleck, contact, or related transformation, reproduces the leading perturbation of U as a first-order perturbation: $\delta E_{00,1}^{(U')} = \delta E_{00,2}^{(U)}$. Using closure, this operator also satisfies the relation in Eq. (8). Therefore, this operator satisfies the requirements for the second-order result, so only partially recovers the third-order shift of Eq. (22) as a second-order shift of Eq. (10), which has no E_{ab} term.

1. Pressure shifts from long-range collisions

The primary application that derived E_a was modeling a nonreactive, long-range collision between a group-1 atom and another atom or molecule. To proceed, let us consider the typical case of a collision between a group-1 atom and a group-18 (noble gas) atom, which has a closed shell, and neglect the nuclear spin of the group-18 atom. Collisions with open-shell atoms or molecules

involve spin interactions between the pair, which may be significant. Consider a group-1 atom at position $\mathbf{x}_a$ and a perturbing particle at position $\mathbf{x}_b = \mathbf{x}_a + \mathbf{R}$ [see Fig. 2 (b)], both in their ground states. For $R = |\mathbf{R}|$ large compared to either ground-state wave function extent, but small enough to neglect retardation effects [36], the leading-order interaction in U is given by a dispersive van der Waals form,

$$U_C = -\mathbf{p}_a \cdot \mathbf{E}_b(\mathbf{x}_a), \tag{23}$$

where, as before, $\mathbf{p}_a = -e\mathbf{r}_a$. Likewise, the field $\mathbf{E}_b(\mathbf{x}_a) = (3\mathbf{nn} - \mathbb{1}) \cdot \mathbf{p}_b/R^3$, but here $\mathbf{p}_b = -e\mathbf{r}_b$ is the instantaneous electric-dipole moment of the group-18 atom and $\mathbf{r}_b$ is the sum of its electron positions relative to its nucleus. Together, this gives

$$U_C = -e^2\left[\frac{\mathbf{r}_a \cdot (3\mathbf{nn} - \mathbb{1}) \cdot \mathbf{r}_b}{R^3}\right] = \frac{e^2}{R^3}(\mathbf{r}_a \cdot \mathbf{r}_b - 3z_a z_b), \tag{24}$$

where the projections $z_a = \mathbf{r}_a \cdot \mathbf{n}$ and $z_b = \mathbf{r}_b \cdot \mathbf{n}$. The first-order perturbation $E^{(U_C)}_{00,1}$ vanishes because $\langle r_a \rangle = \langle z_a \rangle = 0$ from symmetry. Similarly, $\langle 00 \,|\, U_C \,|\, \mu 0 \rangle = 0$ due to spherical symmetry for nS states. Noting again that $\langle n \,|\, z_a^2 \,|\, g \rangle = \frac{1}{3}\langle n \,|\, r_a^2 \,|\, g \rangle$ for nS states, we see that the interaction satisfies Eq. (18). Assuming the second-order perturbation $E^{(U_C)}_{00,2} \neq 0$, all requirements are met for the result of Eq. (22). Rewriting the second-order perturbation as $\delta E^{(U_C)}_{00,2} = -C_6 R^{-6}$, where C_6 is the van der Waals dispersion coefficient of the colliding pair [50–52], we can write the shift as

$$\frac{\delta A_{g,C}}{A_g} \approx -\left(\frac{2}{E_a} + \frac{1}{E_{ab}}\right)\frac{C_6}{R^6}, \tag{25}$$

where the correction energy of Eq. (21) is

$$E_{ab} = -\frac{\langle 00 \,|\, U_C^2 \,|\, 00 \rangle}{\delta E^{(U_C)}_{00,2}} \approx \frac{2e^4 \langle r_a^2 \rangle \langle r_b^2 \rangle}{3\, C_6}, \tag{26}$$

assuming uncorrelated electron positions [30]. Using Eq. (13) and approximating $\langle r_a^2 \rangle \approx \langle r^2 \rangle$, we can rewrite this as

$$E_{ab} \approx \frac{8e^2 \langle r^2 \rangle C_{3,b}}{C_6}, \tag{27}$$

which uses an atom-surface C_3 dispersion coefficient for the collision partner. We estimate the E_{ab} of Eq. (27) in Sec. IV C for pairs of group-1 and group-18 (noble gas) atoms.

2. Stark shift from a static electric field

To test values of the characteristic energies E_a for pressure shifts, Ref. [30] connected E_a with scalar, static Stark shifts. For this application, consider a group-1 atom in a uniform, static electric field $\mathbf{E} = E\mathbf{z}$ aligned with the Cartesian unit vector $\mathbf{z}$ [see Fig. 2 (c)]. The dominant interaction responsible for this shift has the form

$$U_E = -\mathbf{p}_a \cdot \mathbf{E} = eEz_a, \tag{28}$$

where again $\mathbf{p}_a = -e\mathbf{r}_a$ and the projection $z_a = \mathbf{r}_a \cdot \mathbf{z}$. The first-order perturbation $E^{(U_E)}_{00,1}$ vanishes because $\langle z_a \rangle = 0$, and $\langle 00 \,|\, U_E \,|\, \mu 0 \rangle = 0$ for nS states, both from symmetry. Using $\langle n \,|\, z_a^2 \,|\, g \rangle = \frac{1}{3}\langle n \,|\, r_a^2 \,|\, g \rangle$ for nS states, this interaction satisfies Eq. (18). Therefore, assuming the second-order perturbation $E^{(U_E)}_{00,2} \neq 0$, all requirements are met for the third-order shift results. Rewriting the second-order perturbation as $\delta E^{(U_E)}_{00,2} = -\alpha_a(0)E^2/2$, where $\alpha_a(0)$ is the ground-state static

polarizability of the group-1 atom [2,51,53], the intermediate result of Eq. (20) is then

$$\frac{\delta A_{g,E}}{A_g} \approx -\left(\frac{E^2}{2\hat{E}}\right)\left(\frac{4e^2\langle r_a^2\rangle}{3E_a} + \alpha_a(0)\right) \approx -\left(\frac{E^2}{2\hat{E}}\right)\left(\frac{4e^2\langle r^2\rangle}{3E_a} + \alpha_a(0)\right). \tag{29}$$

The resulting hyperfine shift is usually summarized with an isotope-dependent Stark shift coefficient, $k = \delta A_{g,E}(I+\frac{1}{2})/(hE^2)$, which is precisely known for many group-1 atoms due to its connection to BBR shifts in microwave atomic clocks [51].

What remains is to choose a value for the effective energy $\hat{E}$. Reference [30] chose E_P for this value, which is the energy difference between the gS ground state and first excited P state (neglecting fine structure), giving

$$k \approx -\frac{(I+\frac{1}{2})A_g}{2hE_P}\left(\frac{4e^2\langle r^2\rangle}{3E_a} + \alpha_a(0)\right). \tag{30}$$

The motivation for this choice came from using the approximation $E_\mu - E_0 \approx E_P$ and closure with the static polarizability $\alpha_a(0) = -(2/E^2)\delta E_{00,2}^{(U_E)}$, giving $\alpha_a(0) \approx 2e^2\langle r_a^2\rangle/(3E_P) \approx 2e^2\langle r^2\rangle/(3E_P)$, which is accurate to within 6% error for Li but increases to roughly 42% for Cs and 71% for Fr (not 5% for Na–Cs as mistakenly reported in Ref. [30]).

Note that this shift coefficient is of the form of the intermediate result of Eq. (20). Alternatively, the shift coefficient can be put in the form of Eqs. (1) and (22). Using Eq. (21), the energy $E_{ab} \approx 2e^2\langle r_a^2\rangle/[3\alpha_a(0)] \approx E_P$, which then gives

$$k \approx -\frac{(I+\frac{1}{2})A_g\alpha_a(0)}{2h}\left(\frac{2}{E_a} + \frac{1}{E_P}\right). \tag{31}$$

We estimate the coefficients k using both Eqs. (30) and (31) in Sec. IV D for a representative isotope of each group-1 atom.

III. METHODS

We computed the characteristic energies E_a for each group-1 atom and used these energies to estimate the resulting hyperfine shifts for the three applications described above. For convenience, Table V in the Appendix provides many properties of the atoms used in these computations. As summarized below, the computation of E_a and its uncertainty followed the numerical approach of Ref. [30] used previously for Na, K, Rb, and Cs. We revised this approach to provide updated values for those atoms and extended it to provide values for the remaining group-1 atoms H, Li, and Fr. Additionally, to check these numerical results, we estimated E_a using a scaling approach. For nonrelativistic H with no QED corrections (or "textbook" H), this approach is exact and provides a check of the numerical result. For the other atoms, this approach is approximate and comes from adapting the calculation for H, providing a rough check of the similarity noticed between the numerical results and $2E_S$, where $E_S = E_{(g+1)} - E_g$ is the splitting between the ground and first excited nS states.

A. Numerical calculation

To numerically estimate the characteristic energy E_a, we calculated the final expression in Eq. (5). Our approach followed that outlined in Ref. [30], which estimated E_a for Na, K, Rb, and Cs, but not for H, Li, or Fr. This approach is semiempirical in that it uses experimental values where available and extrapolates otherwise, as described below.

For the nS-state energies E_n and the ionization energies E_∞, we used the values available in Ref. [54]. For the coupling coefficients A_n of ^{1}H, we used the experimental values for A_1 and A_2 from Refs. [55,56] and the theoretical values for A_3 to A_8 from Ref. [57]. For the coefficients A_n of the remaining atoms, we used the experimental values for ^{7}Li, ^{23}Na, ^{39}K, ^{87}Rb, ^{133}Cs, ^{210}Fr, and

^{212}Fr available in Ref. [33], which provides more values for Na, K, Rb, and Cs than were previously used by Ref. [30]. For Fr, we combined the values of two isotopes by using those for ^{212}Fr directly and adding additional values from ^{210}Fr after rescaling them using A_g. For K, we excluded A_{11} and above because of their large uncertainties. For Rb and Cs, we excluded new values at very high n where corresponding values of E_n were unavailable. For Rb, we used the value of A_6 from Ref. [58].

To extrapolate E_n to higher n, we computed their corresponding effective quantum numbers

$$n^* = \sqrt{R_\infty/(E_\infty - E_n)}, \tag{32}$$

where R_∞ is the Rydberg constant. These effective quantum numbers are expected to vary as

$$n^* \approx n - \delta_0. \tag{33}$$

This expression is exact for textbook H, with S-state quantum defect $\delta_0 = 0$ [59]. Therefore, we used a linear fit of n^* versus n to extrapolate both n^* and E_n. The fitted values for δ_0 closely matched the expected values for the S-state quantum defects of

$$\delta_0 = g - \sqrt{R_\infty/E_\infty}. \tag{34}$$

Similarly, the coefficients A_n are expected to vary as

$$A_n \propto (n^*)^{-3}, \tag{35}$$

which is exact for textbook H [46]. Therefore, we used a linear fit of $\ln(A_n)$ versus $\ln(n^*)$ to extrapolate A_n. The fitted slope closely matched the expected value of -3 for all atoms except Li, for which A_6 and A_7 were outliers from this scaling. We adjusted the fit coefficients and uncertainties for Li to capture the influence of these outliers.

To calculate the radial matrix elements, we used real-valued, reduced radial wave functions $P_{n0}(r)$, which relate to the spatial wave functions of the nS valence electron as

$$\psi_{n\mathrm{S}}(\mathbf{r}) = \frac{P_{n0}(r)}{2\sqrt{\pi}\, r}. \tag{36}$$

Here, and subsequently, let r be in units of a_0, such that we can set $a_0 \to 1$. Using these radial functions, the matrix elements are equivalent to the integrals

$$\langle n\mathrm{S} \,|\, r^2 \,|\, g\mathrm{S}\rangle = \int_0^\infty P_{n0}(r) P_{g0}(r)\, r^2\, dr. \tag{37}$$

These functions are zero at the origin, $P_{n0}(0) = 0$, and their slopes give the nuclear value as $\psi_{n\mathrm{S}}(0) = (2\sqrt{\pi})^{-1} dP_{n0}(0)/dr$. To match the sign convention of the square-root formula, these nuclear values must be positive, $\psi_{n\mathrm{S}}(0) > 0$, which leads to negative values for all off-diagonal elements ($n \neq g$) calculated using Eq. (37).

To compute these integrals for H, we used the exact, nonrelativistic (or textbook) wave functions [60],

$$P_{n0}(r) = \frac{2re^{-r/n}}{n^{5/2}} L^1_{n-1}\left(\frac{2r}{n}\right), \tag{38}$$

where $L^k_n(x)$ is an associated Laguerre polynomial. For the ground state,

$$P_{10}(r) = 2re^{-r}, \tag{39}$$

which gives $\langle r^2 \rangle = 3a_0^2 = 3$ for H. For all other group-1 atoms, we used tabulated Roothaan-Hartree-Fock (RHF) wave functions and ground-state expectations $\langle r^2 \rangle$ (triple-zeta form if available) [61,62], and constructed Coulomb-approximation (CA) wave functions for the excited states [63]. In the CA, the alkali-metal radial wave functions are proportional to Whittaker W

functions [64] up to normalization, $P_{n0}(r) \propto W_{n^*,1/2}(2r/n^*)$, which are given by the asymptotic series

$$P_{n0}(r) \approx \sum_{q=0}^{p} c_q e^{-r/n^*} r^{n^*-q}, \tag{40}$$

where the coefficients c_q obey the recurrence relation $c_q = c_{q-1}\, n^*(n^*-q)(n^*-q+1)/2q$ [63]. We chose the upper limit p to give the best convergence of the series at $r = 1a_0 = 1$ when E_n was available, and otherwise extrapolated p by noting that it was very nearly equal to n plus a constant offset for large n. To normalize the CA functions, we used a lower bound of $0.1a_0$, such that $\int_{0.1}^{\infty}[P_{n0}(r)]^2\, dr = 1$. To account for the nuclear sign, we used the property $\lim_{r\to 0} \mathrm{sgn}[P_{n0}(r)] = (-1)^{n+g} \lim_{r\to\infty} \mathrm{sgn}[P_{n0}(r)]$ of the CA functions to relate it to the asymptotic sign.

Using these radial functions, we calculated the off-diagonal matrix elements of Eq. (37) up to $n = 35$. To extrapolate these elements to higher n, we used a linear fit to the asymptotic behavior of $\ln(-\langle gS|r^2|nS\rangle)$ versus $\ln(n^*)$ within the region of $n \in [28, 35]$. For more on the scaling of these elements, see the next section.

Together, using these experimental, calculated, and extrapolated values, we computed the energy E_a for each group-1 atom by summing terms up to $n = 500$. To calculate uncertainties for these values, we numerically estimated the contributions from all fitted extrapolations, from the radial integration bounds, and from the nonorthogonality of the CA and RHF functions. The uncertainties also include contributions from the square-root formula [48,65], the isotope dependence of A_n (except for H) [66], and the experimental uncertainty of A_n [33]. However, these uncertainties do not account for approximations in the derivations of formulas with E_a for the three perturbations.

B. Scaling estimation

We analytically calculated the characteristic energy E_a by computing the dimensionless ratio $\mathcal{R} = E_a/2E_S$, which using Eq. (5) is given by the sum

$$\frac{1}{\mathcal{R}} = \frac{2E_S}{E_a} \approx 2\sum_{n>g}^{\infty} \sqrt{\left|\frac{A_n}{A_g}\right|}\left(\frac{E_S}{E_g - E_n}\right)\frac{\langle nS \mid r^2 \mid gS\rangle}{\langle gS \mid r^2 \mid gS\rangle}. \tag{41}$$

Each term in the sum is the product of three dimensionless factors. The first two factors have expected scalings given previously, which are exact for textbook H. Using Eq. (35), the first factor is

$$\sqrt{\left|\frac{A_n}{A_g}\right|} \approx \left(\frac{g^*}{n^*}\right)^{3/2}, \tag{42}$$

where the effective quantum number for the ground state is $g^* = \sqrt{R_\infty/E_\infty}$. An optional improvement that gives slightly better agreement for the heavy alkali metals is to keep the first term, which gives $\sqrt{|A_n/A_g|} \approx \sqrt{|A_{g+1}/A_g|}\,[(g+1)^*/n^*]^{3/2}$. Using Eqs. (33) and (34), the second factor is

$$\frac{E_S}{E_g - E_n} = -\frac{E_{g+1} - E_g}{E_n - E_g} \approx -\frac{1 - [g^*/(g+1)^*]^2}{1 - (g^*/n^*)^2}. \tag{43}$$

The remaining third term of radial matrix elements can be calculated exactly for textbook H. Using the radial functions of Eqs. (38) and (39), the off-diagonal elements are

$$\langle nS \mid r^2 \mid gS\rangle = \int_0^\infty P_{10}(r)\, P_{n0}(r)\, r^2\, dr = \frac{n^{5/2}}{8}\int_0^\infty z^4\, e^{-z(n+1)/2}\, L^1_{n-1}(z)\, dz, \tag{44}$$

where $z = 2r/n$. A more general form of this integral is given in Eq. 7.414(7) of Ref. [67]:

$$\int_0^\infty z^\beta\, e^{-sz}\, L^1_n(z)\, dz = \frac{\Gamma(\beta+1)\Gamma(n+2)}{n!\, s^{\beta+1}}\, {}_2F_1(-n, \beta+1; 2; 1/s), \tag{45}$$

if $\mathrm{Re}(\beta) > -1$ and $\mathrm{Re}(s) > 0$, where ${}_2F_1$ is the ordinary hypergeometric function. When n is a positive integer, this gives

$$\int_0^\infty z^4 e^{-z(n+1)/2} L_{n-1}^1(z)dz = -\frac{256n^2}{(n^2-1)^3}\left(\frac{n-1}{n+1}\right)^n. \tag{46}$$

Combining results, and noting that $\langle r^2\rangle = 3a_0 = 3$, this gives the off-diagonal elements for H as

$$\frac{\langle n\mathrm{S}\,|\,r^2\,|\,g\mathrm{S}\rangle}{\langle g\mathrm{S}\,|\,r^2\,|\,g\mathrm{S}\rangle} = -\frac{32n^{9/2}}{3(n^2-1)^3}\left(\frac{n-1}{n+1}\right)^n \quad (n \neq g). \tag{47}$$

For the alkali metals, while the integrals of approximate radial functions can be evaluated analytically, the resulting expressions are unwieldy. Instead, we proceeded by adapting the result for H to use effective quantum numbers as follows. For the excited state, we directly substituted $n \to n^*$. For the ground state, however, a direct substitution is not straightforward, since $g = 1$ for H. To proceed, we appealed to how different CA/hydrogenic radial matrix elements are often connected by an energy difference factor [cf. Eq. (9) of Ref. [68]] and tried substitutions of the form $E_n - E_g \propto (n)^{-2} - (g)^{-2} \to (n^*)^{-2} - (g^*)^{-2}$, or equivalently, $(n^2-1)/n^2 \to [(n^*)^2 - (g^*)^2]/(n^*g^*)^2$. We found that applying this substitution to the factor $(n^2-1)^3$ in the denominator of Eq. (47) best adapted the relative variation of the elements versus n^* to the alkali metals. Next, we noticed that the numerical results for $\langle (g+1)\mathrm{S}\,|\,r^2\,|\,g\mathrm{S}\rangle/\langle g\mathrm{S}\,|\,r^2\,|\,g\mathrm{S}\rangle \approx -0.7957 \pm 0.0119$, with the exception of Fr, which seems to be an outlier with a value closer to -0.90. Therefore, we normalized that first ratio to the average value of about -0.7957, which gave

$$\frac{\langle n\mathrm{S}\,|\,r^2\,|\,g\mathrm{S}\rangle}{\langle g\mathrm{S}\,|\,r^2\,|\,g\mathrm{S}\rangle} \approx -0.7957\left(\frac{n^*}{g^*+1}\right)^{9/2}\left(\frac{2g^*+1}{(n^*)^2-(g^*)^2}\right)^3\left(\frac{n^*-1}{n^*+1}\right)^{n^*}\left(\frac{g^*+2}{g^*}\right)^{g^*+1} \quad (n \neq g). \tag{48}$$

Finally, using Eqs. (42) and (43), and either Eqs. (47) or (48) with Eq. (41) gives expressions for the ratio $\mathcal{R}$ that are solely functions of g^*. For textbook H, the exact ratio simplifies to

$$\frac{1}{\mathcal{R}} \approx 16\sum_{n=2}^{\infty}\frac{n^5(n-1)^{n-4}}{(n+1)^{n+4}} \quad (g^* = 1), \tag{49}$$

and for the alkali metals, the approximate ratio simplifies to

$$\frac{1}{\mathcal{R}} \approx \left[1.5914\,\frac{(2g^*+1)^4}{(g^*+1)^2}\left(\frac{g^*+2}{g^*}\right)^{g^*+1}\frac{(g^*)^{3/2}}{(g^*+1)^{9/2}}\right]\sum_{k=1}^{\infty}\frac{(g^*+k)^5}{k^4(2g^*+k)^4}\left(\frac{g^*+k-1}{g^*+k+1}\right)^{g^*+k} (g^* \neq 1), \tag{50}$$

where the summation index $k = n^* - g^* = n - g \geqslant 1$.

IV. RESULTS

A. Characteristic energies

Table I summarizes our results for the characteristic energies E_a. Our main results are the numerically calculated values and uncertainties for each group-1 atom. The fractional uncertainty is lowest for Na, around 3%, and highest for Fr, around 25%. In general, the heavier atom uncertainties are dominated by RHF-CA nonorthogonality, which increases with g. This trend captures the estimated sensitivity to radial wave function details, from the greater number of core electrons. For Li, the uncertainty is dominated by an irregular trend in A_n values, as discussed above, and for H, the dominant contributions are the square-root formula and sensitivity to numerical details.

Table I also provides values of the dimensionless ratio $\mathcal{R} = E_a/2E_S$. The ratios using numerically calculated values for E_a agree well with values computed using the exact scaling of Eq. (49) for H

TABLE I. Characteristic energies E_a (eV) of Eqs. (1), (10), and (22) estimated using Eq. (5). The resulting numerically calculated ratios $E_a/2E_S \approx 1$, which we confirmed using scaling argument as shown. We include previously suggested values for E_a for comparison. The values in parentheses are uncertainties in the last digits.

Group-1 atom	H	Li	Na	K	Rb	Cs	Fr
E_a (this work)							
Numerical calculation	22.2(8)	6.53(33)	6.48(20)	5.29(34)	5.06(46)	4.58(60)	4.8(1.1)
Ratio $\mathcal{R} = E_a/(2E_S)$							
Numerical calculation	1.09(4)	0.97(5)	1.02(3)	1.01(7)	1.01(9)	1.00(13)	1.0(2)
Scaling [exact, Eq. (49)]	1.087						
Scaling [approximate, Eq. (50)]		1.038	1.026	0.986	0.977	0.962	0.972
E_a (previous work, [30])							
Numerical calculation			6.55(33)	5.31(28)	5.05(37)	4.59(48)	
Previously suggested values for E_a							
$\overline{E}_e$ of Ref. [2]	11.90	3.62	3.62	2.98	2.88	2.66	
E_∞ [54] following Ref. [19]	13.598	5.392	5.139	4.341	4.177	3.894	4.073

and approximate scaling of Eq. (50) for the alkalis. The scaling result for Li agrees worst with the numerical result, which is expected, given its aforementioned irregular trend of A_n versus n^*. Plots of various quantities comparing numerical and scaling results generated in our code confirm this general pattern of agreement. These plots are included in an online repository, along with our code [44]. A heuristic argument for this agreement with the alkali metals is that in the sum of $1/\mathcal{R}$, the first term contributes about 80% of the total value. In that first term, the energy denominator is E_S, $\sqrt{|A_n/A_g|} \approx 0.5$ for Li–Fr, and the radial ratio is about 0.80. Together, completing the tail sum removes that 0.80 term, leaving $2E_S$ in the denominator. Interestingly, numerically calculating E_a using only CA wave functions (not shown) caused the ratio $\mathcal{R}$ to follow an increasing trend up to $\mathcal{R} \approx 1.25$ for Fr, highlighting its sensitivity to radial wave function details.

For Na–Cs, the updated physical parameters, extrapolations, and minor numerical improvements did not significantly change the results from those previously reported in Ref. [30] (and reproduced in the table). Our updated calculation for Na has smaller uncertainty than the previous result due to improved extrapolation in p for the CA wave functions. For the other alkali metals, we revised our estimate for the uncertainty due to CA-RHF nonorthogonality, to better capture sensitivity to radial function details, which slightly increased the overall uncertainties. In all cases, the numerical results disagree with a previous estimates for $E_a \approx \overline{E}_e$ given in Ref. [2] (and reproduced in the table) by up to a factor of roughly 2. They also differ from the previous estimate $E_a \approx E_\infty$ of Ref. [19] (reproduced in the table), especially for lighter atoms.

TABLE II. Hyperfine shifts of group-1 atoms near conductive surfaces. Values were calculated using Eq. (14) with group-1 atom-surface C_3 coefficients from Ref. [50] and with a distance of $R = 0.1$ μm from the surface. Representative clock frequency shifts are $\delta f_{\text{clock}} = (I + \frac{1}{2})\delta A_g/h$.

Atom	H	Li	Na	K	Rb	Cs	Fr
$(\delta A_g/A_g) \times 10^9$	−0.091(4)	−1.87(10)	−2.33(8)	−4.4(3)	−5.5(5)	−7.5(1.0)	−7(2)
Isotope	^{1}H	^{7}Li	^{23}Na	^{39}K	^{87}Rb	^{133}Cs	^{212}Fr
δf_{clock} (Hz)	−0.129(5)	−1.50(8)	−4.13(13)	−2.04(13)	−37(4)	−52(7)	−372(90)

TABLE III. Energies E_{ab} of expressions (1) and (22) for group-1–group-18 (noble gas) collision pairs. Values were computed using Eq. (27) with values of C_6 from Table G of Ref. [50], of C_3 from Table H of Ref. [50], and of RHF matrix elements $\langle r^2 \rangle$ from Refs. [61,62]. Uncertainties are solely due to C_3 and C_6, where available.

E_{ab} (eV)	He	Ne	Ar	Kr	Xe
H	43.546	55.0(3)	36.15(19)	35.3(3)	33.02(16)
Li	32.37(3)	42.1(2)	24.46(15)	22.99(9)	20.43(10)
Na	33.23(4)	43.0(3)	25.33(13)	23.88(17)	21.30(10)
K	33.24(7)	42.9(3)	25.42(18)	24.06(17)	21.47(13)
Rb	33.61(9)	43.2(3)	25.84(16)	24.58(15)	21.96(12)
Cs	34.2(2)	43.9(4)	26.4(2)	25.14(17)	22.54(17)
Fr	38.4(3)	49.3(5)	30.0(4)	28.7(3)	25.8(3)

B. Wall shifts near surfaces

Table II summarizes calculations of the hyperfine shifts for group-1 atoms due to interaction with a conducting surface at a chosen distance of $R = 0.1$ μm, computed using Eq. (14). The uncertainty is dominated by the uncertainty in E_a, which generally increases with mass. The predicted shifts of a representative clock frequency, $\delta f_{\text{clock}} = (I + \frac{1}{2})\delta A_g/h$, fall in the hertz to tens of hertz range for this distance. Such shifts are resolvable with current techniques, and would be even more so at closer distances R, since they scale with R^{-3}. Note that ^{212}Fr has no "0–0" clock transition; the listed value is representative of the scale of ground-state hyperfine shifts.

C. Pressure shifts during collisions

Table III summarizes values of the correction energies E_{ab} for collisions between group-1 atoms and group-18 (noble gas) atoms. These computed values all satisfy $E_{ab} > E_a/2$, and the E_a term usually dominates over the E_{ab} term in Eq. (1), excluding H. The listed uncertainties are due to the uncertainties of C_3 and C_6 from Ref. [50].

D. Stark shifts in static electric fields

Table IV summarizes calculations of the Stark-shift coefficients k computed using Eqs. (30) and (31). The listed uncertainties are due to E_a alone. The values computed using Eq. (30) all agree, as expected, with previous calculations using the same expression in Ref. [30] and, with the exception of H, with experimental results from Refs. [51,69]. The values computed using

TABLE IV. Stark-shift coefficients k (10^{-10} Hz/(V/m)^2) estimated using Eqs. (30) and (31). The values in parentheses are uncertainties in the last digits, which for this work only include the contributions due to E_a. Experimental values from Refs. [51,69] are included for comparison, as well as a semiempirical value for ^{210}Fr scaled by $A_g(I + \frac{1}{2})$ from Ref. [71].

Atom	^{1}H	^{7}Li	^{23}Na	^{39}K	^{87}Rb	^{133}Cs	^{212}Fr
k (this work)							
Value [using Eq. (30)]:	−0.000 675(12)	−0.0588(11)	−0.121(2)	−0.075(2)	−1.29(5)	−2.50(15)	−10.7(1.3)
Value [using Eq. (31)]:	−0.000 620(10)	−0.0575(11)	−0.1163(14)	−0.069(2)	−1.15(4)	−2.15(11)	−8.3(8)
k (previous work, [30])			−0.120(3)	−0.074(2)	−1.29(4)	−2.50(13)	
k (experimental, [51,69])	−0.000 84(2)	−0.061(2)	−0.124(3)	−0.071(2)	−1.23(3)	−2.271(4)	
k (semiempirical, [71])							−8.47

Eq. (31) are comparable, and more importantly, also agree with experimental results, up to the same exception for H. Therefore, both forms for k are equivalent with respect to the available experimental values and their uncertainties. For the case of H, the mutual disagreement likely stems from neglecting a contribution from continuum states. For H, the discrepancy between our result for k and the measured value matches the roughly 20% contribution to $\alpha_a(0)$ from the continuum that we neglect, mentioned by Ref. [51], compared to approximately 10% for Cs, mentioned by Ref. [70]. For each computed value of k, the fractional contribution of the E_a term in Eq. (30) or (31) was roughly 40%. For Fr, there is no experimental value available, so for comparison, we scaled a semiempirical result computed for ^{210}Fr from Ref. [71] by $(I + \frac{1}{2})A_g$, and the resulting value is consistent with our prediction.

V. DISCUSSION

In Sec. IV, we reported calculations of several experimentally relevant parameters for group-1 atoms perturbed by collisions with group-18 atoms, by static electric fields, or by nearby conducting surfaces. We calculated updated or extended values for the characteristic energy E_a, which appears in ground-state hyperfine shifts in all three of the applications derived above, and likely others. These updated results for E_a are based on numerical sums using experimental measurements where available. Using an exact scaling calculation in the case of textbook H, we validated our numerical approach using the principal-quantum-number dependence of some atomic properties. We adapted this scaling method, using some approximations, to validate the numerical result for the alkali metals, and found good agreement between the two approaches.

Compared to older estimates for the characteristic energy E_a, our results are larger by up to a factor of about 2. For Na–Cs, our results are very close to our prior calculations using the same method [30]. Updated inputs and slight numerical improvements only led to small changes in their values; at the level of estimated uncertainty, there were no significant changes in E_a for Na–Cs.

One surprising result from both our numerical calculations and scaling arguments is that the characteristic energy E_a is close to $2E_S$. In particular, the ratio $E_a/2E_S$ was very nearly unity for all of the alkali metals. This coincidence merits further investigation. From exploring how the ratio changed when using only CA functions instead of CA with RHF functions, we speculate that the fine details of the radial wave functions play an important role in this coincidence.

For long-range collision shifts, our updated and expanded results for E_a and E_{ab} should prove useful to other work investigating pressure shifts and interaction potentials between group-1 and group-18 atoms, such as Refs. [20–23]. They could also potentially have implications for experiments with cold atoms, since the long-range van der Waals potential influences scattering in the vicinity of Feshbach resonances [72], as well as in magnetoassociation [27–29]. Note that to calculate E_{ab} for this application, we had to choose particular values of C_3 and C_6, which influences the values and uncertainty of E_{ab}. For example, we used the values of C_6 reported in Ref. [50], which have $\lesssim$1% fractional uncertainty. Some other methods for evaluating C_6 agree with Ref. [50] within their estimated uncertainties [73], but others differ by up to 5% (with no estimated uncertainties) [74].

For the Stark shift coefficients k, we found good agreement with experimental results for the alkali metals using both the intermediate form of Eq. (20), which follows our previous work [30], and the final form of Eq. (31) that we derived to better match Eq. (1), which used $E_{ab} \approx E_P$. At the level of available uncertainty, these two forms are indistinguishable compared to experiment. The agreement using Eq. (31) is sensitive to the exact choice of E_{ab}: The value of E_P came from using $E_{ab} \approx 2e^2\langle r_a^2\rangle/[3\alpha_a(0)]$ and then $\langle r_a^2\rangle \approx \langle r^2\rangle$. Interestingly, for all atoms, the agreement slightly worsened using $E_{ab} \approx 2e^2\langle r_a^2\rangle/[3\alpha_a(0)]$ directly, and even more so using Eq. (13) to replace $\langle r_a^2\rangle$ with an atom-surface C_3 for the group-1 atom.

A testable prediction of our calculations is the wall shift for group-1 atoms near conducting surfaces. While our derivation assumed a perfect conducting surface, Ref. [75] predicts that the ground-state shifts δE_g of atoms near dielectric and metallic surfaces differ by a factor of order

unity from those near perfect conductors. Thus, the values in Sec. IV B should provide an order-of-magnitude estimate for similar atom-surface interactions near arbitrary surfaces that can be modeled using an effective dielectric constant [75,76]. Using clock transitions in alkali atoms, many of these estimated shifts should be measurable using current techniques for achievable wall distances of $R \approx 0.1$ μm [77]. For vapor cells with antirelaxation coatings, alkali atoms can dwell near the surface, leading to measurable clock shifts [78]. In this case, the shift seems to depend on dwell time, rather than a characteristic distance, indicating a different shift mechanism than described here. The typical atom-surface distance in chip traps is much larger, $R \approx 10$–100 μm [79], and some optical lattice setups trap atoms as close as $R \approx 1$ μm from a window [80], so these shifts should be negligible for most cold-atom experiments. In hollow-core fiber applications, alkali atoms are closer to the fiber surfaces, typically $R \approx 0.1$–10 μm, though the wall shift predicted here would be dominated by other effects [81]. One emerging field where atoms are held much closer to surfaces is in nanostructured slot waveguides [82] or nanograting experiments [83], where the atoms can be $R \approx 50$ nm from the surface. Some research on alkali metals in nanocells probes wall interactions for $R \approx 50$–250 nm [84–89]. The response of an atom to a nearby surface can also be altered using surface plasmon resonances engineered to match an atomic transition frequency [90]. The performance of alkali-atom microwave clocks might be improved using spoof surface plasmons [91] to observe super- or subradiant microwave emission, and potentially improve the performance of microwave clocks, similar to Refs. [92,93]. Future work could use the results in Sec. IV B to evaluate the most promising candidate system for such a scheme.

Another effect of interest to such applications are hyperfine-induced quadrupole moments. Our derivation focused on the Fermi-contact hyperfine interaction of Eq. (2), because the spherical symmetry of nS states suppresses the higher-order terms in the hyperfine interaction. However, such noncontact hyperfine terms are important simultaneous interactions. For the alkali-metal atoms, Ref. [94] calculates how these terms slightly distort the spherical symmetry of the ground state in a way that induces a significant quadrupole moment. If there is an external electric-field gradient at the atom, then this moment shifts the energy and clock frequency. In our calculation of wall shifts, we assumed a perfectly flat surface and thus a negligible spatial gradient. In practice, any sharp features on nearby conducting or dielectric surfaces can drastically enhance the local electric field and its gradient, potentially leading to important shifts from hyperfine-induced quadrupole moments.

Our derivations here require only a modest set of conditions on the form of the interactions, so are fairly general. A similar approach could be useful for extending this work to estimate shifts due to other interactions. The most straightforward are other interactions where $U \propto \langle r^2 \rangle$, but a similar approach could be used with other radial matrix elements, such as different radial powers and/or radial derivatives, likely leading to different versions of corresponding characteristic energies. Possible ways to explore this adaptation would be to modify our numerical code to calculate different elements or to adapt the scaling estimations by using commutator relations to convert them to model different radial elements using the Coulomb approximation [cf. Eq. (9) of Ref. [68]].

VI. CONCLUSION

In this paper, we treated three scenarios that lead to shifts of the ground-state hyperfine coupling in group-1 atoms with the particular form of Eq. (1). We showed how such shifts can arise as either a second-order effect (i.e., surface interactions) or a third-order effect (i.e., collisions and external electric fields). In all cases, a characteristic energy E_a appears that depends only on the properties of the group-1 atom. For third-order shifts, another energy E_{ab} appears that corrects for additional details of the interaction (e.g., choice of collision partner). Using updated experimental values and improved numerical techniques, we calculated E_a, E_{ab} for collisions with group-18 (noble gas) atoms, van der Waals shifts near surfaces, and Stark/BBR shift coefficients k for static electric fields. We found good agreement with experimental results for k, where available, and provided a testable prediction of hyperfine shifts near surfaces.

Our approach provides a straightforward way to estimate various experimentally relevant parameters using a small number of spectroscopic and calculated parameters. This approach should extend to estimate hyperfine shifts for other interactions—our derivations of the shifts made fairly modest assumptions. We expect future work will extend our approach to other interactions and applications.

ACKNOWLEDGMENTS

B.A.O. acknowledges support from the M. J. Murdock Charitable Trust and the National Science Foundation through Grant No. PHY-2418777.

DATA AVAILABILITY

The data that support the findings of this paper are openly available in the Zenodo repository at [96], and an updated version is available in a GitHub repository. The data include MATLAB code that computed the numerical results, example output (text and plots) produced by the code, and a Mathematica notebook that computed scaling results.

APPENDIX: REFERENCE VALUES

Table V provides some reference values used in our calculations for the group-1 atoms.

TABLE V. Reference values for group-1 atoms. Some uncertainties and full-precision values are suppressed for clarity, though calculations used additional precision where applicable. The ground-state principal quantum number g and effective quantum number g^* appear in expressions in Sec. III B. E_D, E_S, and E_∞ are the first excited P- and S-state term energies and the ionization energy, respectively. The value of $\langle gS|r^2|gS\rangle$ for textbook H is exact, while the others are calculated using RHF approximate wave functions. "a.u." denotes atomic units.

Atom	H	Li	Na	K	Rb	Cs	Fr
g	1	2	3	4	5	6	7
$g^* = \sqrt{R_\infty/E_\infty}$	1	1.5885	1.6271	1.7704	1.8048	1.8693	1.8278
E_P (eV) [54]	10.1988	1.8478	2.1037	1.6147	1.5792	1.4317	1.6567
E_S (eV) [54]	10.1988	3.3731	3.1914	2.6070	2.4961	2.2981	2.4474
E_∞ (eV) [54]	13.5984	5.3917	5.1391	4.3407	4.1771	3.8939	4.0727
$\langle gS\|(r/a_0)^2\|gS\rangle$ [61,62]	3	17.7384	20.7048	31.5428	36.1679	44.9530	49.5441
$\alpha_a(0)$ (a.u.) [51,95]	4.5	164.2	162.7	290.8	318.8	401.0	317.8
C_3 atom-surface (a.u.) [50]	0.25	1.512	1.871	2.896	3.426	4.268	4.437
Isotope	^{1}H	^{7}Li	^{23}Na	^{39}K	^{87}Rb	^{133}Cs	^{212}Fr
I	$\frac{1}{2}$	$\frac{3}{2}$	$\frac{3}{2}$	$\frac{3}{2}$	$\frac{3}{2}$	$\frac{7}{2}$	5
A_g/h (MHz) [33]	1420.4058	401.7520	885.8131	230.8599	3417.3413	2298.1579	9064.2

[1] A. Bisht, P. Arora, and V. G. Achanta, Precision timekeeping with atomic clocks: Evolution and future directions, Nat. Commun. **17**, 5284 (2026).
[2] J. Vanier and C. Audoin, *The Quantum Physics of Atomic Frequency Standards* (Hilger, Bristol, 1989).
[3] L. Pezzè, A. Smerzi, M. K. Oberthaler, R. Schmied, and P. Treutlein, Quantum metrology with nonclassical states of atomic ensembles, Rev. Mod. Phys. **90**, 035005 (2018).
[4] M. S. Safronova, D. Budker, D. DeMille, D. F. J. Kimball, A. Derevianko, and C. W. Clark, Search for new physics with atoms and molecules, Rev. Mod. Phys. **90**, 025008 (2018).

[5] L. Cong, W. Ji, P. Fadeev, F. Ficek, M. Jiang, V. V. Flambaum, H. Guan, D. F. Jackson Kimball, M. G. Kozlov, Y. V. Stadnik, and D. Budker, Spin-dependent exotic interactions, Rev. Mod. Phys. **97**, 025005 (2025).
[6] C. Quint, F. Heiße, J. Jaeckel, L. Leimenstoll, C. H. Keitel, and Z. Harman, Stringent constraints on new pseudoscalar and vector bosons from precision hyperfine splitting measurements, Phys. Rev. Lett. **136**, 113001 (2026).
[7] S. G. Karshenboim, Some possibilities for laboratory searches for variations of fundamental constants, Can. J. Phys. **78**, 639 (2000).
[8] X. Yang, S. Wang, S. Wilkins, and R. G. Ruiz, Laser spectroscopy for the study of exotic nuclei, Prog. Part. Nucl. Phys. **129**, 104005 (2023).
[9] J. Du, F. Shi, X. Kong, F. Jelezko, and J. Wrachtrup, Single-molecule scale magnetic resonance spectroscopy using quantum diamond sensors, Rev. Mod. Phys. **96**, 025001 (2024).
[10] J. F. Barry, J. M. Schloss, E. Bauch, M. J. Turner, C. A. Hart, L. M. Pham, and R. L. Walsworth, Sensitivity optimization for NV-diamond magnetometry, Rev. Mod. Phys. **92**, 015004 (2020).
[11] F. A. Zwanenburg, A. S. Dzurak, A. Morello, M. Y. Simmons, L. C. L. Hollenberg, G. Klimeck, S. Rogge, S. N. Coppersmith, and M. A. Eriksson, Silicon quantum electronics, Rev. Mod. Phys. **85**, 961 (2013).
[12] R. Hanson, L. P. Kouwenhoven, J. R. Petta, S. Tarucha, and L. M. K. Vandersypen, Spins in few-electron quantum dots, Rev. Mod. Phys. **79**, 1217 (2007).
[13] A. D. Ludlow, M. M. Boyd, J. Ye, E. Peik, and P. O. Schmidt, Optical atomic clocks, Rev. Mod. Phys. **87**, 637 (2015).
[14] H. Margenau and W. W. Watson, Pressure effects on spectral lines, Rev. Mod. Phys. **8**, 22 (1936).
[15] W. Hindmarsh and J. M. Farr, Collision broadening of spectral lines by neutral atoms, Prog. Quantum Electron. **2**, 141 (1973).
[16] J. Vanier and C. Tomescu, *The Quantum Physics of Atomic Frequency Standards: Recent Developments*, 2nd ed. (CRC Press, Boca Raton, 2025).
[17] J. C. Camparo, Semiempirical theory of Carver rates in alkali/noble-gas systems, J. Chem. Phys. **126**, 244310 (2007).
[18] F. J. Adrian, Matrix effects on the electron spin resonance spectra of trapped hydrogen atoms, J. Chem. Phys. **32**, 972 (1960).
[19] R. Herman and H. Margenau, Frequency shifts in hyperfine splitting of alkalis: A correction, Phys. Rev. **122**, 1204 (1961).
[20] K. Ishikawa, Collisional shifts of hyperfine resonances of ground-state atoms calculated with modified pseudopotential and orthogonalization, Appl. Phys. B **130**, 71 (2024).
[21] K. Ishikawa, Flying characterization of colliding partners by hyperfine splitting frequency of neutral paramagnetic atoms, J. Chem. Phys. **159**, 064303 (2023).
[22] K. Ishikawa, Noble-gas atoms characterized by hyperfine frequency shift of lithium atom, J. Chem. Phys. **156**, 144301 (2022).
[23] K. Ishikawa, Pseudopotential analysis on hyperfine splitting frequency shift of alkali-metal atoms in noble gases, revisited, J. Chem. Phys. **158**, 084306 (2023).
[24] F. Gong, Y.-Y. Jau, and W. Happer, Nonlinear pressure shifts of alkali-metal atoms in inert gases, Phys. Rev. Lett. **100**, 233002 (2008).
[25] B. H. McGuyer, T. Xia, Y.-Y. Jau, and W. Happer, Hyperfine frequencies of ^{87}Rb and ^{133}Cs atoms in Xe gas, Phys. Rev. A **84**, 030501(R) (2011).
[26] B. H. McGuyer, Isotope study of the nonlinear pressure shifts of ^{85}Rb and ^{87}Rb hyperfine resonances in Ar, Kr, and Xe buffer gases, J. Chem. Phys. **158**, 144304 (2023).
[27] K. M. Jones, E. Tiesinga, P. D. Lett, and P. S. Julienne, Ultracold photoassociation spectroscopy: Long-range molecules and atomic scattering, Rev. Mod. Phys. **78**, 483 (2006).
[28] P. S. Żuchowski, J. Aldegunde, and J. M. Hutson, Ultracold RbSr molecules can be formed by magnetoassociation, Phys. Rev. Lett. **105**, 153201 (2010).
[29] D. A. Brue and J. M. Hutson, Magnetically tunable Feshbach resonances in ultracold Li-Yb mixtures, Phys. Rev. Lett. **108**, 043201 (2012).

[30] B. H. McGuyer, Hyperfine-frequency shifts of alkali-metal atoms during long-range collisions, Phys. Rev. A **87**, 054702 (2013).
[31] W. M. Itano, L. L. Lewis, and D. J. Wineland, Shift of $^2S_{1/2}$ hyperfine splittings due to blackbody radiation, Phys. Rev. A **25**, 1233 (1982).
[32] T. Fleig, Variational calculation of the hyperfine Stark effect in atomic ^{87}Rb, ^{133}Cs, and ^{169}Tm, Phys. Rev. A **112**, 052802 (2025).
[33] M. Allegrini, E. Arimondo, and L. A. Orozco, Survey of hyperfine structure measurements in alkali atoms, J. Phys. Chem. Ref. Data **51**, 043102 (2022).
[34] J. E. Lennard-Jones, Processes of adsorption and diffusion on solid surfaces, Trans. Faraday Soc. **28**, 333 (1932).
[35] G. L. Klimchitskaya, U. Mohideen, and V. M. Mostepanenko, The Casimir force between real materials: Experiment and theory, Rev. Mod. Phys. **81**, 1827 (2009).
[36] H. B. G. Casimir and D. Polder, The influence of retardation on the London-van der Waals forces, Phys. Rev. **73**, 360 (1948).
[37] A. Laliotis, B.-S. Lu, M. Ducloy, and D. Wilkowski, Atom-surface physics: A review, AVS Quantum Sci. **3**, 043501 (2021).
[38] Z. Wu, Wall interactions of spin-polarized atoms, Rev. Mod. Phys. **93**, 035006 (2021).
[39] B. Dutta, C. Boldt, G. Garcia-Arellano, M. Ducloy, P. Pedri, S. Scheel, and A. Laliotis, Selective reflection Casimir-Polder spectroscopy in vapor cells: The influence of the thermal velocity distribution, Phys. Rev. A **112**, 012815 (2025).
[40] B. Dutta, J. C. de Aquino Carvalho, G. Garcia-Arellano, P. Pedri, A. Laliotis, C. Boldt, J. Kaushal, and S. Scheel, Effects of higher-order Casimir-Polder interactions on Rydberg atom spectroscopy, Phys. Rev. Res. **6**, L022035 (2024).
[41] B. Dutta, Probing cesium Rydberg atoms close to a sapphire surface, Ph.D. thesis, Sorbonne University, 2024.
[42] B. Debord, F. Amrani, L. Vincetti, F. Gérôme, and F. Benabid, Hollow-core fiber technology: The rising of "gas photonics", Fibers **7**, 16 (2019).
[43] E. Da Ros, N. Cooper, J. Nute, and L. Hackermueller, Cold atoms in micromachined waveguides: A new platform for atom-photon interactions, Phys. Rev. Res. **2**, 033098 (2020).
[44] https://github.com/olsenlab-science/group1-HFS.
[45] B. H. McGuyer, Atomic physics with vapor-cell clocks, Ph.D. thesis, Princeton University, 2012.
[46] E. Arimondo, M. Inguscio, and P. Violino, Experimental determinations of the hyperfine structure in the alkali atoms, Rev. Mod. Phys. **49**, 31 (1977).
[47] M.-A. Bouchiat, Measuring the Fr weak nuclear charge by observing a linear Stark shift with small atomic samples, Phys. Rev. Lett. **100**, 123003 (2008).
[48] V. A. Dzuba and V. V. Flambaum, Off-diagonal hyperfine interaction and parity nonconservation in cesium, Phys. Rev. A **62**, 052101 (2000).
[49] C. Cohen-Tannoudji, B. Diu, and F. Laloë, *Quantum Mechanics, Vol. 2: Angular Momentum, Spin, and Approximation Methods*, 2nd ed., Textbook Physics (Wiley, New York, 2005).
[50] A. Derevianko, S. G. Porsev, and J. F. Babb, Electric dipole polarizabilities at imaginary frequencies for hydrogen, the alkali-metal, alkaline-earth, and noble gas atoms, At. Data Nucl. Data Tables **96**, 323 (2010).
[51] J. Mitroy, M. S. Safronova, and C. W. Clark, Theory and applications of atomic and ionic polarizabilities, J. Phys. B: At. Mol. Opt. Phys. **43**, 202001 (2010).
[52] J.-Y. Zhang and J. Mitroy, Long-range dispersion interactions. I. Formalism for two heteronuclear atoms, Phys. Rev. A **76**, 022705 (2007).
[53] K. D. Bonin and V. V. Kresin, *Electric-Dipole Polarizabilities of Atoms, Molecules, and Clusters* (World Scientific, Singapore, 1997).
[54] A. Kramida, Y. Ralchenko, J. Reader, and NIST ASD Team, NIST Atomic Spectra Database, version 5.12, 2009, https://dx.doi.org/10.18434/T4W30F.
[55] S. G. Karshenboim and V. G. Ivanov, Hyperfine structure in hydrogen and helium ion, Phys. Lett. B **524**, 259 (2002).

[56] R. G. Bullis, C. Rasor, W. L. Tavis, S. A. Johnson, M. R. Weiss, and D. C. Yost, Ramsey spectroscopy of the $^2S_{1/2}$ hyperfine interval in atomic hydrogen, Phys. Rev. Lett. **130**, 203001 (2023).
[57] U. D. Jentschura and V. A. Yerokhin, Quantum electrodynamic corrections to the hyperfine structure of excited S states, Phys. Rev. A **73**, 062503 (2006).
[58] R. Ayachitula, M. D. Anderson, C. D. McLaughlin, R. J. Knize, C. E. Mungan, and M. D. Lindsay, Precision measurement of hyperfine constants and isotope shift of the Rb $^6S_{1/2}$ state via a two-photon transition, Phys. Rev. A **110**, 022803 (2024).
[59] W. Happer, *Optically Pumped Atoms*, 1st ed. (John Wiley & Sons, Incorporated, Weinheim, 2010).
[60] D. J. Griffiths and D. F. Schroeter, *Introduction to Quantum Mechanics*, 3rd ed. (Cambridge University Press, Cambridge, 2018).
[61] C. Bunge, J. Barrientos, and A. Bunge, Roothaan-Hartree-Fock ground-state atomic wave functions: Slater-type orbital expansions and expectation values for $Z = 2$–54, At. Data Nucl. Data Tables **53**, 113 (1993).
[62] A. D. McLean and R. S. McLean, Roothaan-Hartree-Fock atomic wave functions Slater basis-set expansions for $Z = 55$–92, At. Data Nucl. Data Tables **26**, 197 (1981).
[63] P. J. Oreto, Y.-Y. Jau, A. B. Post, N. N. Kuzma, and W. Happer, Buffer-gas-induced shift and broadening of hyperfine resonances in alkali-metal vapors, Phys. Rev. A **69**, 042716 (2004).
[64] F. W. J. Olver, D. W. Lozier, R. F. Boisvert, and C. W. Clark, *NIST Handbook of Mathematical Functions* (Cambridge University Press, Cambridge, England, 2010).
[65] C. Bouchiat and C. Piketty, Magnetic dipole and electric quadrupole amplitudes induced by the hyperfine interaction in the cesium 6S-7S transition and the parity violation calibration, J. Phys. **49**, 1851 (1988).
[66] J. Persson, Table of hyperfine anomaly in atomic systems—2023, At. Data Nucl. Data Tables **154**, 101589 (2023).
[67] I. S. Gradštejn, J. M. Ryžik, A. Jeffrey, D. Zwillinger, and I. S. Gradštejn, *Table of Integrals, Series and Products*, 7th ed. (Elsevier Academic Press, Amsterdam, 2009).
[68] M. L. Sánchez, B. Moreno, and A. López Piñeiro, Matrix-element calculations for hydrogenlike atoms, Phys. Rev. A **46**, 6908 (1992).
[69] J. G. Stuart, D. J. Larson, and N. F. Ramsey, Differential Stark shifts in the hydrogen maser, Phys. Rev. A **22**, 2092 (1980).
[70] E. J. Angstmann, V. A. Dzuba, and V. V. Flambaum, Frequency shift of the cesium clock transition due to blackbody radiation, Phys. Rev. Lett. **97**, 040802 (2006).
[71] T. Aoki, R. Sreekantham, B. K. Sahoo, B. Arora, A. Kastberg, T. Sato, H. Ikeda, N. Okamoto, Y. Torii, T. Hayamizu, *et al.*, Quantum sensing of the electron electric dipole moment using ultracold entangled Fr atoms, Quantum Sci. Technol. **6**, 044008 (2021).
[72] C. Chin, R. Grimm, P. Julienne, and E. Tiesinga, Feshbach resonances in ultracold gases, Rev. Mod. Phys. **82**, 1225 (2010).
[73] D.-H. Zhang, Y.-B. Xu, J. Jiang, L. Jiang, L.-Y. Xie, and C.-Z. Dong, Long-range dispersion interactions between excited states of K and rare-gas atoms, J. Phys.: Conf. Ser. **875**, 082008 (2017).
[74] B. Eshel, J. A. Cardoza, D. E. Weeks, and G. P. Perram, Role of adiabaticity in controlling alkali-metal fine-structure mixing induced by rare gases, Phys. Rev. A **95**, 042708 (2017).
[75] J. M. Wylie and J. E. Sipe, Quantum electrodynamics near an interface, Phys. Rev. A **30**, 1185 (1984).
[76] M. Fichet, F. Schuller, D. Bloch, and M. Ducloy, Van der Waals interactions between excited-state atoms and dispersive dielectric surfaces, Phys. Rev. A **51**, 1553 (1995).
[77] Y. Balland, L. Absil, and F. Pereira Dos Santos, Quectonewton local force sensor, Phys. Rev. Lett. **133**, 113403 (2024).
[78] E. P. Corsini, T. Karaulanov, M. Balabas, and D. Budker, Hyperfine frequency shift and Zeeman relaxation in alkali-metal-vapor cells with antirelaxation alkene coating, Phys. Rev. A **87**, 022901 (2013).
[79] J. Fortágh and C. Zimmermann, Magnetic microtraps for ultracold atoms, Rev. Mod. Phys. **79**, 235 (2007).
[80] C. Gross and W. S. Bakr, Quantum gas microscopy for single atom and spin detection, Nat. Phys. **17**, 1316 (2021).

[81] S. Okaba, T. Takano, F. Benabid, T. Bradley, L. Vincetti, Z. Maizelis, V. Yampol'skii, F. Nori, and H. Katori, Lamb-Dicke spectroscopy of atoms in a hollow-core photonic crystal fibre, Nat. Commun. **5**, 4096 (2014).

[82] R. Ritter, N. Gruhler, H. Dobbertin, H. Kübler, S. Scheel, W. Pernice, T. Pfau, and R. Löw, Coupling thermal atomic vapor to slot waveguides, Phys. Rev. X **8**, 021032 (2018).

[83] J. Lecoffre, A. Hadi, M. Bruneau, C. Garcion, N. Fabre, É. Charron, N. Gaaloul, G. Dutier, and Q. Bouton, Measurement of Casimir-Polder interaction for slow atoms through a material grating, Phys. Rev. Res. **7**, 013232 (2025).

[84] K. A. Whittaker, J. Keaveney, I. G. Hughes, A. Sargsyan, D. Sarkisyan, and C. S. Adams, Spectroscopic detection of atom-surface interactions in an atomic-vapor layer with nanoscale thickness, Phys. Rev. A **92**, 052706 (2015).

[85] A. Sargsyan, A. Gogyan, and D. Sarkisyan, Features of the van der Waals interaction on the cesium $^6S_{1/2} \rightarrow {}^7P_{3/2}$ transition in an optical nanocell, Spectrochim. Acta, Part B **239**, 107493 (2026).

[86] A. Sargsyan, Study of the interaction of rubidium atoms with sapphire surface using spectroscopic nanocells, J. Appl. Spectrosc. **90**, 731 (2023).

[87] A. Sargsyan, R. Momier, C. Leroy, and D. Sarkisyan, Competing van der Waals and dipole-dipole interactions in optical nanocells at thicknesses below 100 nm, Phys. Lett. A **483**, 129069 (2023).

[88] A. Sargsyan, E. Klinger, R. Boudot, and D. Sarkisyan, Doppler-free spectroscopy of the Cs $^6S_{1/2} - {}^7P_{3/2}$ atomic transition at 456 nm in a nanometric-thick vapor layer, Opt. Lett. **50**, 3229 (2025).

[89] A. D. Sargsyan and D. H. Sarkisyan, Study of the van der Waals effect in potassium atomic vapours, J. Contemp. Phys. (Arm. Acad. Sci.) **60**, 261 (2025).

[90] E. A. Chan, S. A. Aljunid, G. Adamo, A. Laliotis, M. Ducloy, and D. Wilkowski, Tailoring optical metamaterials to tune the atom-surface Casimir-Polder interaction, Sci. Adv. **4**, eaao4223 (2018).

[91] F. J. Garcia-Vidal, A. I. Fernández-Domínguez, L. Martin-Moreno, H. C. Zhang, W. Tang, R. Peng, and T. J. Cui, Spoof surface plasmon photonics, Rev. Mod. Phys. **94**, 025004 (2022).

[92] M. A. Norcia, J. R. K. Cline, J. A. Muniz, J. M. Robinson, R. B. Hutson, A. Goban, G. E. Marti, J. Ye, and J. K. Thompson, Frequency measurements of superradiance from the strontium clock transition, Phys. Rev. X **8**, 021036 (2018).

[93] M. O. Araújo, J. C. D. A. Carvalho, P. W. Courteille, and A. Laliotis, Cooperative atomic emission from a line of atoms interacting with a resonant plane surface, Phys. Rev. A **110**, 032813 (2024).

[94] A. Derevianko, Hyperfine-induced quadrupole moments of alkali-metal-atom ground states and their implications for atomic clocks, Phys. Rev. A **93**, 012503 (2016).

[95] D. Baye, Exact nonrelativistic polarizabilities of the hydrogen atom with the Lagrange-mesh method, Phys. Rev. A **86**, 062514 (2012).

[96] B. A. Olsen, Estimating the ground-state hyperfine shifts of group-1 atoms due to long-range collisions, static electric fields, and nearby surfaces, Zenodo, 2026, https://doi.org/10.5281/zenodo.22149598.